Time-dependent density functional approach for the calculation of inelastic x-ray scattering spectra of molecules

Arto Sakko, Angel Rubio, Mikko Hakala, and Keijo Hämäläinen

Citation: J. Chem. Phys. **133**, 174111 (2010); doi: 10.1063/1.3503594

View online: http://dx.doi.org/10.1063/1.3503594

View Table of Contents: http://jcp.aip.org/resource/1/JCPSA6/v133/i17

Published by the American Institute of Physics.

Time-dependent density functional approach for the calculation of inelastic x-ray scattering spectra of molecules

Arto Sakko,[1,a)] Angel Rubio,[2] Mikko Hakala,[1] and Keijo Hämäläinen[1]
[1]*Department of Physics, University of Helsinki, P.O. Box 64, Helsinki FI-00014, Finland*
[2]*Nano-Bio Spectroscopy Group and ETSF Scientific Development Centre, Departamento Física de Materiales, Universidad del País Vasco, Centro de Física de Materiales CSIC-UPV/EHU-MPC and DIPC, Av. Tolosa 72, San Sebastián E-20018, Spain*

(Received 6 July 2010; accepted 27 September 2010; published online 2 November 2010)

We apply time-dependent density functional theory to study the valence electron excitations of molecules and generalize the typically used time-propagation scheme and Casida's method to calculate the full wavevector dependent response function. This allows the computational study of dipole-forbidden valence electron transitions and the dispersion of spectral weight as a function of the wavevector. The method provides a novel analysis tool for spectroscopic methods such as inelastic x-ray scattering and electron energy loss spectroscopy. We present results for benzene and CF_3Cl and make a comparison with experimental results. © *2010 American Institute of Physics*. [doi:10.1063/1.3503594]

I. INTRODUCTION

Time-dependent density functional theory (TDDFT) has become a widely used tool for the simulation of the electronic structure underlying the physical and chemical properties of a wide range of different materials from low-dimensional nanostructures to complex extended systems.[1] TDDFT is frequently used, for example, to model the photoabsorption spectrum which is governed by the dipole allowed transitions of valence electrons to the unoccupied electronic states. In this work we demonstrate the applicability of TDDFT to nondipole valence electron transitions in molecules, translating the concept of momentum dependent inverse dielectric function of solids to finite systems.[2] From the experimental point of view, these transitions are often studied using electron energy loss spectroscopy (EELS), but the work here is also strongly motivated by the ongoing development in synchrotron radiation based techniques that now enable the experimental survey of dipole forbidden transitions with unprecedented energy resolution and statistical accuracy.[3–6] Combination of reliable computational methods and high-resolution spectroscopy provides a detailed picture of the electronic structure and dynamics in molecular materials.

Inelastic x-ray scattering (IXS) is a bulk-sensitive method for studying elementary excitations, such as phonons and electronic excitations. It allows the experimental determination of the inverse macroscopic dielectric function with various advantages compared to the complementary techniques such as photoabsorption and electron energy loss spectroscopy. In particular, the experiments are not restricted to dipole transitions and can be carried out at extreme sample environments.[7] The experimental spectrum contains a wealth of information on various physical phenomena related to the microscopic structure of the material. For instance, because of the wide range of accessible energy and momentum transfers (or, equivalently, wavevectors), IXS is often used for probing the dispersion of phonons in crystalline materials.[8] It also enables the study of valence electron excitations and it has been used to measure, e.g., valence plasmon dispersion in superconductors.[9] Plasmonics attracts general interest of a wide scientific community,[10] and the knowledge of the plasmon properties in small nanostructures has important applications.[11,12] Another promising IXS based technique is the imaging of the time-dependent electron dynamics.[13–15] This intriguing method demonstrates how IXS can provide information on very small time (as) and length (Å) scales. A comprehensive explanation of the theory, experiments and the applications of IXS can be found in Ref. 16.

The most thorough interpretation of the measured IXS spectrum often requires comparison with calculations, and therefore various computational methods for the electronic structure have been employed for simulating the spectrum. The most sophisticated methods such as configuration interaction and quantum Monte Carlo are also computationally the heaviest and can usually be applied only to small molecules. In contrast, TDDFT offers a good compromise between computational cost and accuracy.[17] It has been successfully applied to analyze the IXS spectra of solids as well as liquids.[15,18,19] The present work demonstrates that TDDFT can be used to quantitatively simulate the IXS spectrum of molecules, as illustrated for the case of benzene and CF_3Cl. The calculations here are carried out within adiabatic local density approximation (ALDA), but the method itself is general and therefore also other exchange correlation potentials can be employed. The presented method is applicable for various materials ranging from small molecules and nanoscale structures to liquids and has remarkable potential for future work in modern x-ray physics.

[a)]Electronic mail: arto.sakko@helsinki.fi.

II. METHOD

TDDFT is a generalization of the static density functional theory (DFT) to cover the electronic excitations and other time-dependent phenomena.[1,20] There are several equivalent approaches for using TDDFT in the calculation of the response functions that are related to the experimentally measurable excitation spectra, and in this work we concentrate on two of them: the Casida's method[21] (CM) and the time propagation method (TPM).[22] The other approaches are described in detail in Ref. 1. The theoretical framework is presented here for finite systems, but the corresponding formalism for extended systems as well as the connection to molecules can be found, e.g., in Ref. 2.

CM has its roots in time-dependent Hartree–Fock theory[23] and it can be formulated as a matrix equation for calculating the transition rates and energies. It is especially convenient for simulating the discrete, i.e., bound-to-bound transitions in small molecules. However, due to the different scaling of the computational cost with respect to the system size, TPM is more suitable for larger systems. In TPM the electronic structure is propagated in time under the influence of an external electric field and the induced charge fluctuations describe the response of the system to this perturbation. This allows the simulation of the discrete transitions and often within good accuracy also the excitations above the ionization threshold, i.e., transitions to the electronic states in the continuum.[24] It can be used to study both linear and nonlinear response functions and also the response of the system in the nonperturbative region.[25,26] It also enables a straightforward study of the combined electron-ion dynamics.[27]

In an IXS experiment one measures the double differential cross section which is within the first Born approximation given by

$$\frac{d^2\sigma}{d\omega d\Omega} = \left(\frac{d\sigma}{d\Omega}\right)_{Th} S(\mathbf{q},\omega), \tag{1}$$

where $\left(\frac{d\sigma}{d\Omega}\right)_{Th}$ is the Thomson scattering cross section and $S(\mathbf{q},\omega)$ is the dynamic structure factor of the material. The transferred momentum and energy from the electromagnetic field to the sample are $\mathbf{q}$ and ω, respectively. We use atomic units in this work, except when providing numerical values to compare with available experimental data. The dynamic structure factor is closely connected to the inverse macroscopic dielectric function

$$S(\mathbf{q},\omega) = \frac{-q^2}{4\pi^2 n}\mathrm{Im}\left[\frac{1}{\varepsilon_M(\mathbf{q},\omega)}\right], \tag{2}$$

where n is the average electron density of the system. This connection implies that when $S(\mathbf{q},\omega)$ is determined, the full dielectric function $\varepsilon_M(\mathbf{q},\omega)$ can be obtained using Kramers–Kronig relations.[28]

Dynamic structure factor and thereby the inelastic x-ray scattering spectrum are closely related to the density-density response function $\chi(\mathbf{r},\mathbf{r}',t-t')$ of the material, which connects a weak time-dependent external field $V_{\mathrm{ext}}(\mathbf{r},t)$ to the charge density fluctuation $\Delta\rho(\mathbf{r},t)$ that the field induces

$$\Delta\rho(\mathbf{r},t) = \int_{-\infty}^{t} dt' \int d^3\mathbf{r}'\chi(\mathbf{r},\mathbf{r}',t-t')V_{\mathrm{ext}}(\mathbf{r}',t'). \tag{3}$$

From the fluctuation-dissipation theorem[28] it follows that

$$S(\mathbf{q},\omega) = \frac{-1}{\pi}\mathrm{Im}[\chi(\mathbf{q},-\mathbf{q},\omega)]. \tag{4}$$

Equation (3) is given in time (t) and space ($\mathbf{r}$) coordinates, from which one can change to momentum ($\mathbf{q}$) and frequency (ω) representation by Fourier transformations.

Density-density response function is also closely connected to the molecular polarizability tensor $\alpha_{ij}(\omega)$ which can be probed experimentally using photoabsorption spectroscopy.[29] At low momentum transfer the dynamic structure factor of molecular systems (but not of extended ones, see Ref. 2) is proportional to the photoabsorption spectrum. When momentum transfer increases the IXS and photoabsorption spectra begin to differ due to the increasing contribution of nondipole transition channels. The $\mathbf{q}$-dependent transition rates are often characterized using the so-called generalized oscillator strength, which is defined for a given discrete transition m as

$$\mathrm{GOS}(q,\omega_m) = \frac{2\omega_m}{q^2}\int \frac{d\Omega_q}{4\pi} S(\mathbf{q},\omega_m), \tag{5}$$

where the angular integration implies the directional average of momentum transfer vectors over the solid angle.[30]

A. Casida's method

The starting point in the CM is the calculation of one-electron eigenstates $\phi_{j\sigma}(\mathbf{r})$ and energy eigenvalues $\varepsilon_{j\sigma}$ of the occupied and unoccupied electronic states using time-independent DFT (σ is the spin index). Thereafter, using the time-dependent Kohn–Sham equations one can cast the problem of finding the transition rates and energies into the matrix equation[21]

$$\sum_{m'} \hat{R}_{mm'}\mathbf{F}_{m'} = \omega^2\mathbf{F}_m, \tag{6}$$

where

$$\hat{R}_{mm'} = (\varepsilon_{f\sigma}-\varepsilon_{i\sigma})^2\delta_{mm'} + 2\sqrt{\varepsilon_{f\sigma}-\varepsilon_{i\sigma}}K_{mm'}\sqrt{\varepsilon_{f'\sigma'}-\varepsilon_{i'\sigma'}} \tag{7}$$

and $m=(i,f,\sigma)$ label the electron-hole pairs [occupied orbital $\phi_{i\sigma}(\mathbf{r})$ and unoccupied orbital $\phi_{f\sigma}(\mathbf{r})$]. $K_{mm'}$ is the electron-hole interaction matrix element

$$K_{(i,f,\sigma),(i',f',\sigma')} = \int d^3\mathbf{r}\int d^3\mathbf{r}'\phi^*_{f\sigma}(\mathbf{r})\phi_{i\sigma}(\mathbf{r})\times\left[\frac{1}{|\mathbf{r}-\mathbf{r}'|} + f_{\mathrm{xc}}(\mathbf{r},\mathbf{r}')\right]\times\phi_{f'\sigma'}(\mathbf{r}')\phi^*_{i'\sigma'}(\mathbf{r}'), \tag{8}$$

and f_{xc} is the nonlocal frequency-independent exchange-correlation kernel. Casida's equation couples the different electron-hole excitations and thus goes beyond the single particle picture. Its solution provides the real valued excitation energies ω_I, and the transition rates are calculated from

the eigenvectors $\mathbf{F}_I$. The expression for the dynamic structure factor is

$$S(\mathbf{q},\omega) = \sum_I |\mathbf{M}^\dagger(\mathbf{q}) S^{-1/2} \mathbf{F}_I|^2 \delta(\omega - \omega_I), \tag{9}$$

where $M_{(i,f,\sigma)}(\mathbf{q}) = \int d^3\mathbf{r}\, \phi^*_{i\sigma}(\mathbf{r}) e^{-i\mathbf{q}\cdot\mathbf{r}} \phi_{f\sigma}(\mathbf{r})$, $S_{(i,f,\sigma),(i',f',\sigma')} = \frac{\delta_{\sigma\sigma'}\delta_{ii'}\delta_{ff'}}{(n_{i\sigma}-n_{f\sigma})(\varepsilon_{i\sigma}-\varepsilon_{f\sigma})}$, and $n_{i\sigma}$ and $n_{f\sigma}$ are the occupation numbers of the Kohn–Sham orbitals $\phi_{i\sigma}(\mathbf{r})$ and $\phi_{f\sigma}(\mathbf{r})$, respectively.

B. Time propagation method

Starting from any arbitrary initial state for the electronic structure, time propagation formulation of TDDFT provides in principle the exact dynamical evolution of the system. In our case we address the $\mathbf{q}$-dependent response function starting from the electronic ground state. Therefore the TPM requires first the calculation of the ground state electron density using time-independent DFT, which corresponds to the situation at times $t<0$. At $t=0$ a sudden external field $V_{\text{ext}}(\mathbf{r},t) = I_0 \delta(t) e^{i\mathbf{q}\cdot\mathbf{r}}$ is applied.[31] If I_0 is sufficiently weak the induced charge density is determined by the density-density response function through Eq. (3). The Fourier transform of the resulting induced charge density is

$$\Delta\rho(\mathbf{q},\omega) = I_0 \int_{-\infty}^{\infty} dt e^{-i\omega t} \int d^3\mathbf{r} \int d^3\mathbf{r}'\, e^{-i\mathbf{q}\cdot\mathbf{r}} \chi(\mathbf{r},\mathbf{r}',t) e^{i\mathbf{q}\cdot\mathbf{r}'}. \tag{10}$$

On the right hand side appears the density-density response function in $(\mathbf{q},\omega)$-space. Therefore, combining Eqs. (4) and (10) one can write

$$S(\mathbf{q},\omega) = \frac{-1}{\pi I_0} \text{Im}[\Delta\rho(\mathbf{q},\omega)]. \tag{11}$$

The scheme for calculating $S(\mathbf{q},\omega)$ can be thus laid out as

(1) Calculate ground state electron density.
(2) Perturb the system with an external potential $V_{\text{ext}}(\mathbf{r},t) = I_0\delta(t)e^{i\mathbf{q}\cdot\mathbf{r}}$.
(3) Propagate the system with time-dependent Kohn–Sham equations.
(4) Calculate the Fourier-transform of the induced charge density and apply Eq. (11) to determine $S(\mathbf{q},\omega)$.

To prevent the necessity of using a complex-valued external potential that leads to nonunitary time evolution, the calculation is carried out in two steps. In the first one, a sine-shaped potential $(I_0\delta(t)\sin(\mathbf{q}\cdot\mathbf{r}))$ is applied, and in the second a cosine-shaped one $(I_0\delta(t)\cos(\mathbf{q}\cdot\mathbf{r}))$. These give the induced charge densities $\Delta\rho_{\sin}(\mathbf{r},t)$ and $\Delta\rho_{\cos}(\mathbf{r},t)$, respectively, and the charge density induced by the $e^{i\mathbf{q}\cdot\mathbf{r}}$-shaped field is obtained as

$$\Delta\rho(\mathbf{r},t) = \Delta\rho_{\cos}(\mathbf{r},t) + i\Delta\rho_{\sin}(\mathbf{r},t). \tag{12}$$

With isotropic samples, such as gases and liquids, the IXS measurement provides the directionally averaged dynamic structure factor $S(q,\omega) = \frac{1}{4\pi}\int d\Omega_{\mathbf{q}} S(\mathbf{q},\omega)$. It can be calculated using a set of $\mathbf{q}$-vectors that lie at a sphere of radius q. These vectors can be generated using Gauss–Legendre quadrature scheme for spherical integration.[32] However, a more appealing option is obtained by using the expression $e^{i\mathbf{q}\cdot\mathbf{r}} = 4\pi\sum_{l=0}^{\infty}\sum_{m=-l}^{l} i^l j_l(qr) Y_{lm}(\hat{\mathbf{q}}) Y_{lm}(\hat{\mathbf{r}})$ and writing

$$\frac{1}{4\pi}\int d\Omega_{\mathbf{q}} \chi(\mathbf{r},\mathbf{r}',t) e^{-i\mathbf{q}\cdot\mathbf{r}} e^{i\mathbf{q}\cdot\mathbf{r}'} = 4\pi \sum_{l=0}^{\infty}\sum_{m=-l}^{l} \chi(\mathbf{r},\mathbf{r}',t) j_l(qr) j_l(qr') Y_{lm}(\hat{\mathbf{r}}) Y_{lm}(\hat{\mathbf{r}}'), \tag{13}$$

where $j_l(qr)$ and $Y_{lm}(\hat{\mathbf{r}})$ are the spherical Bessel function and real spherical harmonic, respectively. Thus, instead of the exponential external perturbation one performs a set of calculations with different angular momentum quantum numbers l and m, where the external perturbation is $V^{lm}_{\text{ext}}(\mathbf{r},t) = I_0\delta(t) j_l(qr) Y_{lm}(\hat{\mathbf{r}})$. From each of these calculations, indexed by the numbers l and m, one calculates

$$\Delta\rho_{lm}(q,t) = \int d^3\mathbf{r} \Delta\rho(\mathbf{r},t) j_l(qr) Y_{lm}(\hat{\mathbf{r}}). \tag{14}$$

Then the directionally averaged dynamic structure factor is

$$S(q,\omega) \approx \frac{-4}{I_0} \times \text{Im}\left[\sum_{l=0}^{L_{\max}}\sum_{m=-l}^{l} \int_0^{\infty} dt e^{-i\omega t} \Delta\rho_{lm}(q,t)\right], \tag{15}$$

where the finite value for $L_{\max}$ is due to the truncation of the originally infinite series. At the limit of low momentum transfer only the terms with $l=1$, i.e., dipole allowed transitions, contribute. Thus in this case the directional average requires only three calculations, which is consistent with the photoabsorption spectrum calculation.[22] When q increases more terms must be included and Eq. (15) provides a systematic way to improve the average. A straightforward approach is to increase $L_{\max}$ until the f-sum rule is satisfied within required accuracy. The series also gives a direct way to discriminate between different transition channels, i.e., terms with different l, that contribute to the dynamic structure factor. This advantageous feature was originally demonstrated in various pioneering IXS studies.[33–36] A similar analysis was recently demonstrated for IXS from valence excitations of NiO and CoO.[37] In the case of core electron excitations the approach enables the probing of the symmetry properties of specific unoccupied electronic states.[38,39]

III. CALCULATIONS

The calculations are carried out using the OCTOPUS computer code where the q-dependent versions of the TPM and CM were implemented in this work.[40,41] We demonstrate the use of TPM and CM for benzene and CF_3Cl molecules, and make a comparison of the two methods in both cases. In all the calculations the electronic structure is solved in a real space grid employing the finite difference method and zero boundary conditions. The inner shell $(1s)$ electrons are treated using Troullier–Martins norm-conserving pseudopotentials, and the exchange and correlation is included within ALDA. We use approximated enforced time-reversal symmetry propagator with the time step of 1.316 as for benzene and 0.658 as for CF_3Cl for carrying out the time propagation of the electronic structure. All the spectra are convoluted

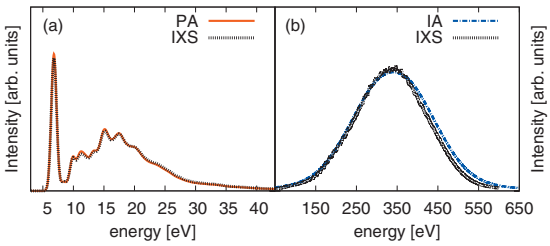

FIG. 1. (a) Low-q and (b) high-q limits of the IXS spectrum correspond to photoabsorption (PA) spectrum and the energy loss spectrum within impulse approximation (IA), respectively. The IXS calculations were carried out with TPM using q-vector along the x-axis and the PA spectrum corresponds to $\mathrm{Im}[\alpha_{xx}(\omega)]$. The polarizability tensor was calculated using OCTOPUS(Refs. 40 and 41) with the same grid as for IXS calculation, and the IA calculation was carried out using a method and computer codes described in Ref. 43.

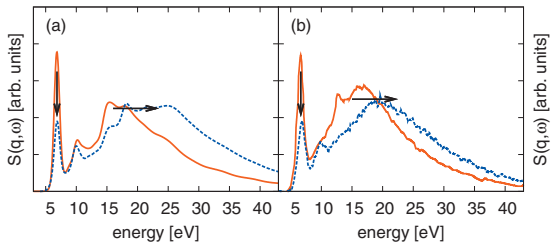

FIG. 2. Dynamic structure factor of gaseous benzene from (a) TPM calculation and (b) EELS experiment. The momentum transfers of the calculated spectra are 0.57 Å^{-1} (solid red curve) and 1.13 Å^{-1} (dashed blue curve). The experimental EELS spectra (from Ref. 44) are gathered at scattering angles of 2.0° (solid red curve) and 4.0° (dashed blue curve) that approximately correspond to the momentum transfers used in the calculation. The arrows indicate two spectral features whose q-dependency is correctly reproduced by the calculation.

using Gaussian line shape with full width at half maximum (FWHM) of 1.0 eV.

Benzene molecule is a typical system for benchmark calculations and also in this work we use it to demonstrate the q-dependent behavior of the dynamic structure factor calculated within TPM and CM. In our calculations the molecule is positioned in the xy plane at the center of a spherically shaped real space grid using equidistant spacing of 0.20 Å between the grid points.[42] In the CM calculation the radius of the grid is 9.0 Å and 160 unoccupied electronic states are used. In the TPM calculation the radius is 7.0 Å and in this case we add an extra absorbing layer with the width of 5.0 Å to the calculation grid, so that the total grid has a radius of 12 Å. Within the layer a complex valued external potential

$$V_{\mathrm{abs}}(r) = -10.0 \times i \times \sin\left(\frac{\pi}{2} \times \frac{r - 7.0\ \text{Å}}{5.0\ \text{Å}}\right)^2\ \text{eV} \qquad (16)$$

is added to the Hamiltonian. It removes part of the excited electrons from the system during the time propagation and thus the absorbing layer mimics the ionization process.[24]

We first demonstrate the behavior of the calculated dynamic structure factor at very low and high momentum transfers. Momentum transfers of 0.19 and 9.45 Å^{-1} along the x-axis are used in these calculations. In the low-q calculation the time propagation lasts for 6.6 fs and in the high-q case the maximum time is 0.66 fs. At low momentum transfers one probes only dipole allowed transitions and the same information as from photoabsorption spectrum is obtained. When momentum transfer increases, also quadrupole and other high order transitions contribute. At the other limit, i.e., when $q \to \infty$, the dynamic structure factor is dominated by the Compton peak at energy $q^2/2$ (340 eV for $q=9.45$ Å^{-1}) as the impulse approximation (IA) becomes valid.[16] These features are demonstrated in Fig. 1.

After having obtained the correct limits of $S(\mathbf{q},\omega)$ at low and high momentum transfers, we next demonstrate that the calculations at the intermediate values for q show similar behavior as observed in an EELS experiment for gaseous benzene,[44] see Fig. 2. In these calculations the maximum time of the propagation is 6.6 fs and the directional averaging is carried out using Eq. (15) with $L_{\max}=4$. The q-dependent behavior is correctly reproduced by the calculation. In particular, the relative intensity of the $\pi-\pi^*$ transition at 7 eV decreases as q increases, and the spectral weight moves toward higher energy. These features are indicated by the arrows in the figure. ALDA is known to provide good results for dipole excitation spectrum of benzene molecule,[45] and our results confirm this also in a wider momentum transfer regime. The reason for the good performance is that the low-energy part of benzene spectrum is dominated by localized single-particle excitations which in general are handled accurately within ALDA and generalized gradient approximation functionals.[46] Most of the discrepancies between experiment and calculation occur above the ionization potential (9.8 eV in the experimental spectrum), in which region the calculation produces too pronounced features. The discrepancies can be mostly attributed to the incorrect asymptotic behavior of ALDA and the lack of proper treatment of the lifetime effects. In particular, the incorrect asymptotic behavior in DFT yields inaccurate high-lying excitation energies.[46,47] Various solutions to this problem, such as the self-interaction[48] and exact-exchange corrections,[49] have been proposed and often provide significant improvements. The finite lifetime effects are approximated in this work by using the absorbing layer. Nevertheless, strong features are still found in the continuum part of the spectrum because the layer is incapable of correctly damping the electronic density fluctuations. Including the lifetime effects properly would require the use of a nonadiabatic functional. Altogether, despite its shortcomings ALDA is clearly well suited for simulating the excitations of molecular benzene. For systems where different kind of transitions (such as excitons, charge-transfer excitations, or double excitations) would contribute, one should use more sophisticated (nonlocal, nonadiabatic, or asymptotically corrected) functionals.[50–52] Because the presented method is independent of the used functional, it can be straightforwardly applied with these functionals.

The separation of the directionally averaged spectrum to various angular momentum components is demonstrated in Fig. 3. It confirms that at low momentum transfer the spectrum mostly reflects the terms with $l=1$. As expected, when q increases and the dipole forbidden transitions enhance, also other transition channels ($l=0,2,3$) contribute significantly.[53]

Freon molecules are widely studied molecules because of their relevance in earth science. Their valence electronic structure plays an important role in their chemical reactivity

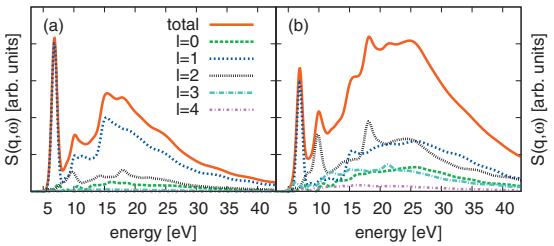

FIG. 3. Separation of the directionally averaged dynamic structure factor of gaseous benzene into different transition channels at momentum transfers of (a) 0.57 Å^{-1} and (b) 1.13 Å^{-1}. At low momentum transfer the dipole selection rule dominates but when the momentum transfer increases, also nondipole transitions give a significant contribution.

and photodissociation processes in the atmosphere. CF_3Cl, i.e., freon-13, is known to have a dipole forbidden transition in its valence spectrum at 7.7 eV[54,55] and therefore it serves as a good benchmark system for the calculation scheme presented in this work.

As was previously described for benzene, also here the molecule is positioned in the center of a spherically shaped real space grid.[56] The radius of the grid is 8.0 Å and the spacing between the grid points 0.12 Å. For the calculation of the dynamic structure factor with CM, 80 unoccupied electronic states are used. The propagation time with TPM is 6.6 fs. The directional averaging is carried out using a set of **q**-vectors generated by the fifth order spherical Gauss–Legendre quadrature scheme.[32]

Figure 4 shows the dynamic structure factor in the vicinity of the first valence electron transitions at various momentum transfer values, calculated using CM. The calculation correctly reproduces the dipole-forbidden transition (7.6 eV) at finite values of q. Figure 4 also shows a comparison of the computational and experimentally measured[55] GOS curves of the 7.6 eV transition. A good overall agreement is achieved and the minor differences could be linked to the use of the LDA kernel in the calculation.

Finally we make a comparison between TPM and CM for benzene and CF_3Cl molecules at intermediate momentum transfer region, see Fig. 5. For benzene the directional averaging of momentum transfer vectors is used and for CF_3Cl **q** is parallel to the C–F bond. Both TPM and CM produce similar spectra for the first few transitions, but at higher energies the results differ significantly. This can be attributed to the finite number of unoccupied electronic states used in the CM which obscures its use at wider energy range. While CM

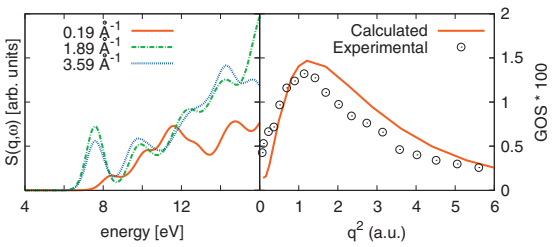

FIG. 4. Calculated IXS spectrum (left) of CF_3Cl demonstrates the momentum transfer dependency of $S(\mathbf{q},\omega)$ and in particular the enhancing of the dipole-forbidden quadrupole-allowed transition at 7.6 eV as q increases. The generalized oscillator strengths (right) calculated with CM for the 7.6 eV transition are shown with experimental (Ref. 55) result.

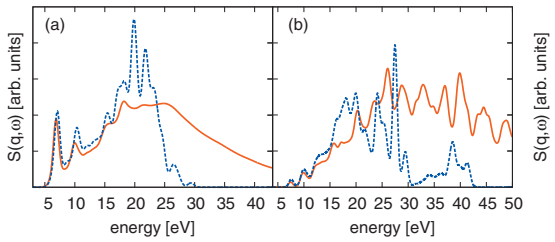

FIG. 5. IXS spectrum of (a) benzene at q=1.13 Å^{-1} (directionally averaged) and (b) CF_3Cl at q=1.89 Å^{-1} (parallel to the C–F bond) calculated using TPM (solid red curves) and CM (dashed blue curves).

is more efficient for calculating transition rates for individual electronic excitations, the advantage of TPM is that it does not require the calculation of the unoccupied states. The corresponding information of the excited states is included in the time evolution. Since the number of necessary unoccupied states can be very large in CM, TPM is often favored especially for large molecules and nanostructures. The convergence of spectral features with CM can be challenging already for relatively small systems if the unoccupied states near ionization threshold play important role in the transitions. This is the case also for benzene for which a significant number of unoccupied states is necessary. TPM does not suffer from the same convergence problems but it can also be computationally heavy if many time steps are required. This is the case if a very high energy resolution is required (the energy resolution of the calculated spectrum is determined by the maximum propagation time, FWHM=$2\pi/T_{\max}$) or if the time step is very small (for instance, when propagating also the inner shell electron states).

IV. CONCLUSIONS AND DISCUSSION

This work illustrates the performance of TDDFT for the calculation of the dynamic structure factor of finite systems as a function of the momentum transfer. CM provides a powerful tool to extract generalized oscillator strengths for specific transitions in small molecules. TPM is more suitable especially for larger systems, but also for smaller ones when one is interested in the spectrum over a wide energy range, or if the CM calculation requires a significant number of unoccupied states. The presented approach for directional averaging allows to distinguish between different transition channels that contribute to the spectrum of isotropic materials. Altogether the presented methods enable a detailed analysis of the inelastic x-ray scattering and electron energy loss spectra. The potential systems where they can be applied include molecules, polymers, liquids as well as nanostructures.

We explicitly demonstrated how the calculated IXS spectrum connects to the photoabsorption cross section at low momentum transfer, and how the Compton peak forms at very high momentum transfer. Between these extreme cases our calculations demonstrate two effects that are probed by varying the momentum transfer. First, dipole-forbidden transitions are observed and enhanced in the calculated spectrum at finite q. These transitions can play important role in, e.g., atmospheric chemistry, where the molecules are excited by energetic electrons and end up in

metastable or dissociative states.[54,55] Second, the calculations show the systematic dispersion of spectral weight that is also observed experimentally, as illustrated for benzene.

At the intermediate momentum transfer region the method can provide new information on, e.g., plasmon dispersion. More generally, the evolution of spectral features as a function of q can be related to the electron density correlations in the system at very short time and length scales. The real-space real-time formalism, as used in this work, provides valuable insight into the electron dynamics.[13,15]

Our calculations for benzene and CF_3Cl were carried out using ALDA which is a reliable approximation especially for the bound single-electron transitions. The presented methods are independent of the exchange-correlation functional and therefore allow also calculations with, e.g., nonlocal and asymptotically corrected functionals. Using a more sophisticated functional could provide further improvement for the excitation spectrum and allow the simulation of other kind of electronic excitations, such as excitons and charge-transfer type transitions.

ACKNOWLEDGMENTS

We acknowledge the Jenny and Antti Wihuri Foundation, Vilho, Yrjö and Kalle Väisälä Foundation, HPC-Europa2 program, Academy of Finland (1127462, Centers of Excellence Program 2006–2011, and National Graduate School in Materials Physics) for financial support, and CSC-IT Center for Science Ltd for computational resources. A.R. acknowledges Spanish MEC (FIS2007-65702-C02-01), ACI-Promociona (ACI2009-1036), Grupos Consolidados UPV/EHU del Gobierno Vasco (IT-319-07), the European Union through e-13 ETSF (Contract No. 211956), and THEMA (Contract No. 228539) projects, as well as the support by the Red Española de Supercomputación and ARINA.

[1] *Time-Dependent Density Functional Theory*, edited by M. A. L. Marques, C. A. Ullrich, F. Nogueira, A. Rubio, K. Burke, and E. K. U. Gross (Springer, Heidelberg, 2006).
[2] F. Sottile, F. Bruneval, A. G. Marinopoulos, L. K. Dash, S. Botti, V. Olevano, N. Vast, A. Rubio, and L. Reining, Int. J. Quantum Chem. **102**, 684 (2005).
[3] M. Minzer, J. A. Bradley, R. Musgrave, G. T. Seidler, and A. Skilton, Rev. Sci. Instrum. **79**, 086101 (2008).
[4] B. P. Xie, L. F. Zhu, K. Yang, B. Zhou, N. Hiraoka, Y. Q. Cai, Y. Yao, C. Q. Wu, E. L. Wang, and D. L. Feng, Phys. Rev. A **82**, 032501 (2010).
[5] R. Verbeni, T. Pylkkänen, S. Huotari, L. Simonelli, G. Vankó, K. Martel, C. Henriquet, and G. Monaco, J. Synchrotron Radiat. **16**, 469 (2009).
[6] J. A. Bradley, G. T. Seidler, G. Cooper, M. Vos, A. P. Hitchcock, A. P. Sorini, C. Schlimmer, and K. P. Nagle, Phys. Rev. Lett. **105**, 053202 (2010).
[7] U. Bergmann, P. Glatzel, and S. P. Cramer, Microchem. J. **71**, 221 (2002).
[8] E. Burkel, J. Phys.: Condens. Matter **13**, 7627 (2001).
[9] S. Galambosi, J. A. Soininen, A. Mattila, S. Huotari, S. Manninen, Gy. Vankó, N. D. Zhigadlo, J. Karpinski, and K. Hämäläinen, Phys. Rev. B **71**, 060504 (2005).
[10] R. P. Van Duyne, Science **306**, 985 (2004).
[11] A. Yurtsever, M. Weyland, and D. A. Muller, Appl. Phys. Lett. **89**, 151920 (2006).
[12] P. A. Midgley and R. E. Dunin-Borkowski, Nature Mater. **8**, 271 (2009).
[13] P. Abbamonte, K. D. Finkelstein, M. D. Collins, and S. M. Gruner, Phys. Rev. Lett. **92**, 237401 (2004).
[14] P. Abbamonte, T. Graber, J. P. Reed, S. Smadici, C.-L. Yeh, A. Shukla, J.-P. Rueff, and W. Ku, Proc. Natl. Acad. Sci. U.S.A. **105**, 12159 (2008).
[15] I. Tavernelli, Phys. Rev. B **73**, 094204 (2006).
[16] W. Schülke, *Electron Dynamics by Inelastic X-Ray Scattering* (Oxford University Press, Oxford, 2007).
[17] K. Burke, J. Werschnik, and E. K. U. Gross, J. Chem. Phys. **123**, 062206 (2005).
[18] A. A. Quong and A. G. Eguiluz, Phys. Rev. Lett. **70**, 3955 (1993).
[19] H.-Ch. Weissker, J. Serrano, S. Huotari, F. Bruneval, F. Sottile, G. Monaco, M. Krisch, V. Olevano, and L. Reining, Phys. Rev. Lett. **97**, 237602 (2006).
[20] E. Runge and E. K. U. Gross, Phys. Rev. Lett. **52**, 997 (1984).
[21] M. E. Casida, in *Recent Advances in Computational Chemistry*, Recent Advances in Density Functional Methods, edited by D. P. Chong (World Scientific, Singapore, 1995), Vol. 1.
[22] K. Yabana and G. F. Bertsch, Phys. Rev. B **54**, 4484 (1996).
[23] P. Jorgensen, Annu. Rev. Phys. Chem. **26**, 359 (1975).
[24] T. Nakatsukasa and K. Yabana, J. Chem. Phys. **114**, 2550 (2001).
[25] Y. Takimoto, F. D. Vila, and J. J. Rehr, J. Chem. Phys. **127**, 154114 (2007).
[26] A. S. de Wijn, S. Kümmel, and M. Lein, J. Comput. Phys. **226**, 89 (2007).
[27] J. L. Alonso, X. Andrade, P. Echenique, F. Falceto, D. Prada-Gracia, and A. Rubio, Phys. Rev. Lett. **101**, 096403 (2008).
[28] D. Pines and P. Nozières, *The Theory of Quantum Liquids* (Benjamin, New York, 1996).
[29] D. Foerster and P. Koval, J. Chem. Phys. **131**, 044103 (2009).
[30] H. Hayashi, N. Watanabe, Y. Udagawa, and C.-C. Kao, Proc. Natl. Acad. Sci. U.S.A. **97**, 6204 (2000).
[31] P. Romaniello and P. L. de Boeij, Phys. Rev. B **71**, 155108 (2005).
[32] K. Atkinson, J. Aust. Math. Soc. Ser. B, Appl. Math. **23**, 332 (1982).
[33] J. R. Fields, P. C. Gibbons, and S. E. Schnatterly, Phys. Rev. Lett. **38**, 430 (1977).
[34] J. M. Auerhammer and P. Rez, Phys. Rev. B **40**, 2024 (1989).
[35] M. H. Krisch, F. Sette, C. Masciovecchio, and R. Verbeni, Phys. Rev. Lett. **78**, 2843 (1997).
[36] K. Hämäläinen, S. Galambosi, J. A. Soininen, Eric L. Shirley, J.-P. Rueff, and A. Shukla, Phys. Rev. B **65**, 155111 (2002).
[37] M. W. Haverkort, A. Tanaka, L. H. Tjeng, and G. A. Sawatzky, Phys. Rev. Lett. **99**, 257401 (2007).
[38] J. A. Soininen, A. Mattila, J. J. Rehr, S. Galambosi, and K. Hämäläinen, J. Phys.: Condens. Matter **18**, 7327 (2006).
[39] A. Sakko, M. Hakala, J. A. Soininen, and K. Hämäläinen, Phys. Rev. B **76**, 205115 (2007).
[40] A. Castro, H. Appel, M. Oliveira, C. A. Rozzi, X. Andrade, F. Lorenzen, M. A. L. Marques, E. K. U. Gross, and A. Rubio, Phys. Status Solidi B **243**, 2465 (2006).
[41] See www.tddft.org/programs/octopus for the program homepage.
[42] Carbon atoms are located at Cartesian coordinates $(0.0, \pm 1.396, 0.0)$ Å and $(\pm 1.209, \pm 0.698, 0.0)$ Å, and the C–H bond length is 1.083 Å.
[43] M. Hakala, S. Huotari, K. Hämäläinen, S. Manninen, Ph. Wernet, A. Nilsson, and L. G. M. Pettersson, Phys. Rev. B **70**, 125413 (2004).
[44] H. M. Boechat-Roberty, M. L. M. Rocco, C. A. Lucas, and G. G. B. de Souza, J. Phys. B **37**, 1467 (2004).
[45] K. Yabana and G. F. Bertsch, Int. J. Quantum Chem. **75**, 55 (1999).
[46] M. Casida, C. Jamorski, K. Casida, and D. Salahub, J. Chem. Phys. **108**, 4439 (1998).
[47] O. Lehtonen, D. Sundholm, R. Send, and M. P. Johansson, J. Chem. Phys. **131**, 024301 (2009).
[48] J. P. Perdew and A. Zunger, Phys. Rev. B **23**, 5048 (1981).
[49] M. Städele, J. A. Majewski, P. Vogl, and A. Görling, Phys. Rev. Lett. **79**, 2089 (1997).
[50] Y.-H. Kim and A. Görling, Phys. Rev. Lett. **89**, 096402 (2002).
[51] A. Hesselmann, A. Ipatov, and A. Görling, Phys. Rev. A **80**, 012507 (2009).
[52] P. Romaniello, D. Sangalli, J. A. Berger, F. Sottile, L. G. Molinari, L. Reining, and G. Onida, J. Chem. Phys. **130**, 044108 (2009).
[53] With $L_{max}=4$ the f-sum rule was obeyed within 5% accuracy.
[54] J. F. Ying, C. P. Mathers, K. T. Leung, H. P. Pritchard, C. Winstead, and V. McKoy, Chem. Phys. Lett. **212**, 289 (1993).
[55] K. T. Leung, J. Electron Spectrosc. Relat. Phenom. **100**, 237 (1999).
[56] We use C–Cl and C–F bond lengths of 1. 824 and 1.342 Å, respectively, and F–C–F angle of 106.7°.